FOREX Publication
Open Access | Rapid and quality publishing

International Journal of
Electrical and Electronics Research (IJEER)
Research Article | Volume 13, Issue 2 | Pages 371-380 | e-ISSN: 2347-470X

Designing Smart Perturb and Observe MPPT Controller for 150W Off-Grid PV System

Raghad Ali Mejeed
Department of Electrical Power and Machines, Collage of Engineering, University of Diyala, 32001 Diyala, Iraq; dr.raghadaljourni@gmail.com

***Correspondence:** *Raghad Ali Mejeed; dr.murtagha2000@gmail.com*

ABSTRACT- Studying the introduction design of a stand-alone solar photovoltaic (PV) system with a disturbance-and-observation (P&O)-based algorithm for maximum power point tracking (MPPT) is an important topic for improving the performance of solar energy systems. The efficient energy system is designed by using solar photovoltaic panels consisting of a number of cells, using P and O algorithms for effective tracking of maximum power, and performing comparative analysis using the traditional model without the MPPT algorithm. In this approach, the terminal voltage of the photovoltaic cell is always set according to the MPP voltage and duty cycle setting directly in the system. The control loop and calculations have been simplified to reduce the time needed to adjust the console gain. The system has a solar panel, MPPT (maximum power point tracking) with controller, DC converter, and a single-phase VSI (voltage source inverter). The proposed system was simulated using MATLAB/Simulink model.

Keywords: Photovoltaic Cells Generator (PVG), Maximum Power Point Tracking (MPPT), perturbs and observes (P&O) Controller, Single Phase VSI (Voltage Source Reflector).

ARTICLE INFORMATION
Author(s): Raghad Ali Mejeed;
Received: 20/02/2025; **Accepted**: 12/06/2025; **Published**: 30/06/2025;
E- ISSN: 2347-470X;
Paper Id: IJEER 2002-06;
Citation: 10.37391/ijeer.130222
Webpage-link:
https://ijeer.forexjournal.co.in/archive/volume-13/ijeer-130222.html

Publisher's Note: FOREX Publication stays neutral with regard to jurisdictional claims in Published maps and institutional affiliations.

1. INTRODUCTION

At this time, sustained forces are generally used in almost all business applications. Due to their special qualities, these powers are delegated to clean, maintainable and inexhaustible supplies, unlike petroleum derivatives that have greatly affected the climate. With such forces, energy states directed toward the Sun are the most sought-after energy source. Despite this advantage, not all systems are ideal as PV systems are sensitive to changes in heat and radiation. To replace in this matter, some methods or algorithms are used to separate the largest force from the PVG that was directed at work, depending on the complexity of the algorithm. The MPPT approach is considered the most typical and applies the P&O control model, in addition to smart technologies to achieve the best performance. As artificial intelligence algorithms and smart technologies have permeated every part of life, micro-grids powered by inverters that construct the grid through a transformer connected to clean energy sources or unlimited distribution energy resources (DERs) have advanced significantly in recent years [1-4]. The load-side electrical connection is the most often used technique for solar energy systems. In this manner, a new circuit breaker or circuit breaker is installed in the electrical panel. A two-pole or two-space circuit breaker will be located in the location farthest from the main breaker. The wires of the solar PV system are then connected to this new solar crusher. Reliance on solar energy is affected by changing climate conditions and day and night restrictions, which also change within the available limits. It is also power enabled that the main structures can support each other through independent charging as well as cleaning the batteries depending on the charge level and the connection point of the solar cell array at which point the battery supply is depleted and also de-boosted. Part of the key solution to the problem of impurities in powered sources is energy storage. By manipulating power, power can be exchanged in an organized manner in running the board against the stretch target in that borderline unit might potentially act as a dedicated dynamic and fast power source, providing an additional read in power to commanders. Self-determination provides this skill to control their own distributions, manage their evaluation further, and supervise the control and encouragement of the flow of energy from the matrix. Different sources can be found in relation to microgrids or in a power dispersal system in relation to the electrical grid. *Figure 1* shows a demonstration chart of the stand-alone SAPV system with MPPT inverter [5-10].

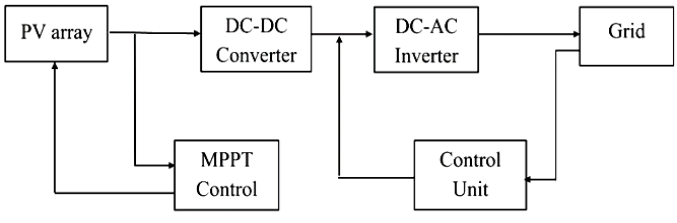

Figure 1. Demonstration diagram of the stand-alone SAPV system using MPPT inverter [5-10]

Thus, a maximum power point tracker, or MPPT, is an electronic DC to DC converter that improves the alignment of the utility grid, battery bank, or solar array (photovoltaic panels). Maximum Power Point Tracking, or MPPT for short, is a system that regulates the amount of charge in your battery

FOREX Publication
Open Access | Rapid and quality publishing
International Journal of Electrical and Electronics Research (IJEER)
Research Article | Volume 13, Issue 2 | Pages 371-380 | e-ISSN: 2347-470X

bank. The gearbox of an automobile is analogous to the operation of an MPPT charge controller. Incorrect gearing of the gearbox does not optimize wheel power. On other words, MPPT examines the PV module's output, compares it to the battery voltage and then determines the best power the PV module can produce to charge the battery and converts it to the best voltage to get maximum current into the battery. Additionally, it might power a DC load that is linked straight to the battery [6–12]. This study used a smart frame to supply the resistive load over the length of the DCDC converter, allowing it to identify the maximum mark offered by the GPV design. The suggested smart system managed significant fluctuations in input PV power by utilizing deep learning algorithms. Potential versus current are inputs in a deep learning network diagram, while the duty cycle is the output [8-14].

This section uses mathematical formulas and graphical graphics to address the fundamental theoretical ideas of solar array control using artificial neural networks (ANNs). With examples of real-world applications and graphics, the fundamentals of photovoltaic functioning will be thoroughly covered. Additionally, typical DC to AC boost controller types will be described with the help of characteristic diagrams and corresponding operational relationships. Lastly, a thorough scientific analysis and explanation of the ANN controller's structure will be provided.

1.1. Photo Voltaic Cells Power Supply

A uniform mass of sun-absorbing glass sheets makes up the solar board. Then, a collection of photovoltaic (PV) units is built using electronic cells, a type of photovoltaic array, which convert sunlight towards a steady DC value. The array is made up of parallel series of cells, each of which is made up of units connected in an integral series. This block enables us to model pre-selected PV modules versus PV modules we choose using the System Advisor Model (2018), National Renewable Energy Laboratory (NREL). As shown in *figure 2* [4-6], the PV array block is a five-parameter model that generates the radiation- and heat-dependent I-V characteristics of the modules by using a light-generated current source (IL), a diode, a series resistance (Rs), and a shunt resistance (Rsh). For a given module, the following equations form the stated I-V diode properties:

$$I_d = I_o e^{\frac{V_d}{V_T}} - 1 \quad (1)$$

$$V_T = \frac{KT}{q} \times nl \times N_{cell} \quad (2)$$

The system's vital power source, which will generate the network against the required power, will be these PV cells. The following is an example of such a unit: A parallel-attached PV array is constructed across a number of PV modules. Each series is made up of units connected in series. Using the NREL System Advisor simulate, this unit enables the simulation of a user-defined PV module against a range of pre-selected PV modules. Sunlight radiation in W/m^2 is input number one, while cell heat in degrees Celsius is input number two.

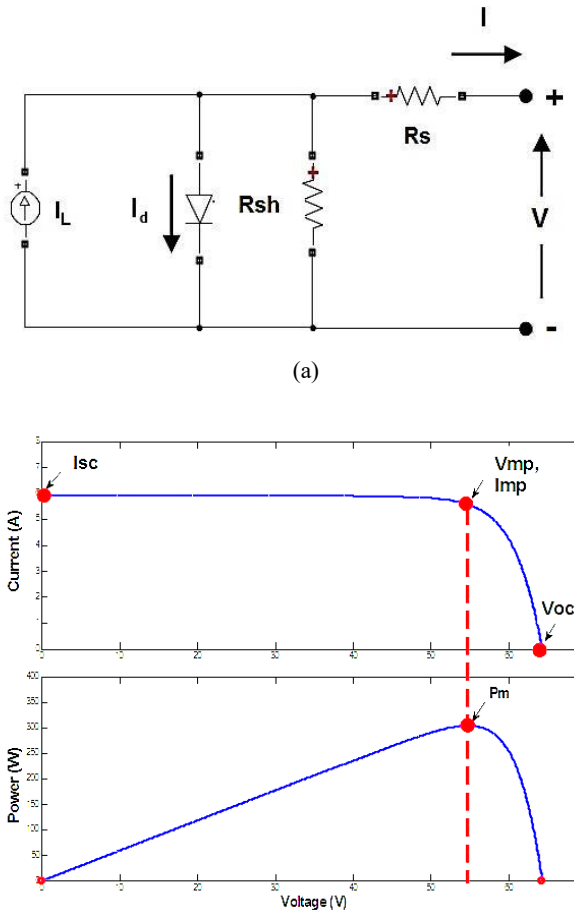

Figure 2. Specifications of the PV cell, (a) equivalent circuit for the PV cell, and (b) characteristics of the PV cell's power and current [6-12]

1.2. Power DC to AC Inverter

Inverters might be considered as a demonstration of a classy of devices named power electronics such controls the electrical power flow. Essentially, by quickly changing the direction of the DC input, the inverter converts DC to AC. This causes the DC input to give rise to the AC output waveform. *Figure 3* displays a common DC-to-AC converter. To acquire the appropriate pulsing operation, there are a number of different methods and strategies that may be found in publications. The most crucial aspect of performing converted AC voltage signal quality is the switching procedure.

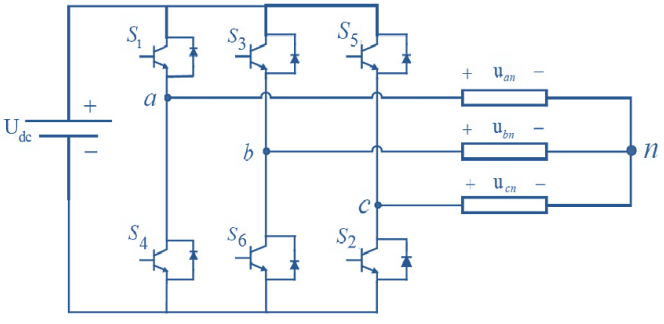

Figure 3. A typical DC-to-AC inverter circuit diagram [6-15]

FOREX Publication
Open Access | Rapid and quality publishing
International Journal of Electrical and Electronics Research (IJEER)
Research Article | Volume 13, Issue 2 | Pages 371-380 | e-ISSN: 2347-470X

Neutral Point Clamped (NPC) inverters are typically used in the efficient design of DC to AC inverters. These inverters are a class of multi-level transducers that employ stabilization diodes to guarantee appropriate voltage distribution among the power switches. *Figure 4* shows the circuit diagram for NPC adapters or inverters.

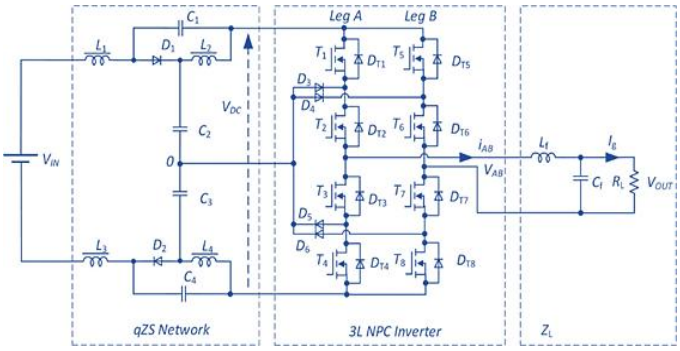

Figure 4. The NPC inverters circuit diagram [6-18]

The quality of the DC to AC signal translation is largely dependent on the choice of inverter switch controller. Advanced research is interested in altering the switching time widths to produce changing width pulses that reduce total harmonic distortion (THD), as the high switching pulses will cause THD in the produced AC signal.

1.3. The Boost DC Power Converter Circuit

Boost converters are designed to raise the voltage of an alternating solar board to a higher, more stable DC voltage. Voltage feedback is used to keep the final voltage constant. To maximize the DC supply voltage and maintain a steady amount of DC power available to the system, this portion is crucial. *Figure 5* shows the Boost Dc Power Converter unit's circuit design as constructed using the MatLab2023b Simulink model.

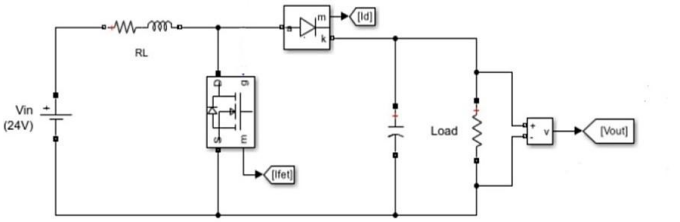

Figure 5. The boost converter circuit, employed with MatLab2023b Simulink

The boost converter attaches the PV arrays to the DC to AC inverter also works to enhance the DC potential while preventing or limiting its fluctuations in order to get the ideal DC quantity for AC conversion preparations. Maximum point power tracking (MPPT) may be achieved by managing the boost converter utilizing a range of techniques and controllers to deliver the best DC potential response along the PV cells. In the parts that follow, we'll talk about the MPPT notion using typical applied controllers. Optimizing DC to AC inverters often involves using an MPPT controller, which stands for optimal maximum power point tracking. Even if the photovoltaic cells' voltage or current is decreased, these controls are used to get the maximum output. The PV arrays' MPPT response is seen in *figure 6* [14–26].

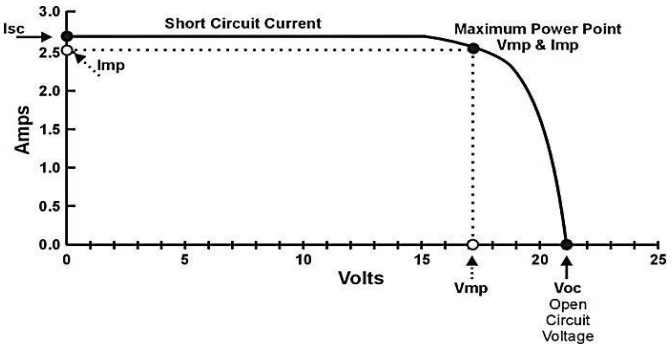

Figure 6. MPPT performance for PV panels [14-26]

Numerous types of MPPT controllers, including voltage source converter (VSC) controllers, artificial neural network (ANN) controllers, and perturb and disturb (P&O) controllers, are accessible in the literature. All of these controllers help the boost converter circuit operate at its best MPPT. In a separate section, the MPPT boost controllers will be thoroughly explained and shown to help you grasp their characteristics and working principles.

1.3.1. Perturb and Disturb (P&O) Controller

For the MPPT approach, this is the most common type of boost controller that is offered. In P&O and IP&O, there are a few MPPT approaches accessible. The P&O method, which is the simplest, periodically moves from the operating point to the maximum power point in order to raise or lower the voltages of the PV cells. In *figure 7*, a standard P&O controller is shown [13-29].

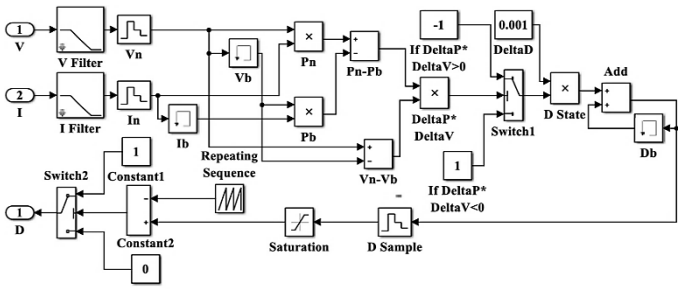

Figure7. A typical P&O controller circuit diagram [13-28]

Using this method, a little disturbance was introduced to generate the PV module's power alternation. Periodically, the photovoltaic resultant energy is calculated and compared to the previous energy. Similar operations continue if the resultant energy is increased; if not, the disturbance is reversed. The following formula might be used to evaluate the resultant current, *I*:

$$v(t) = V_p.e^{(\omega t+\theta_0)} \quad (3)$$

Where; $I_L = I_{ph}$, which is the photocurrent, V, is the resulting voltage, I_D is the parallel diode current, R_{sh} represents the shunt

FOREX Publication
Open Access | Rapid and quality publishing
International Journal of Electrical and Electronics Research (IJEER)
Research Article | Volume 13, Issue 2 | Pages 371-380 | e-ISSN: 2347-470X

resistance, I_{sh} is the shunt current, R_s corresponds to the series resistance, and I_s, is the yield current. Also, the PV saturation current is obtained by:

$$I_S = I_{rs}\left(\frac{T_{op}}{T_{ref}}\right)^3\left[e^{\left(\frac{q\partial_G}{Ak}\left(\frac{1}{T_{op}}-\frac{1}{T_{ref}}\right)\right)}\right] \quad (4)$$

Whereas, the inverted saturation current is represented as:

$$I_{rs} = \frac{I_{sh}}{\left[e^{\frac{V_{dc}}{A.N_s V_T}}-1\right]} \quad (5)$$

Furthermore, the PV equivalent equation photon current might be expressed such as:

$$I_{ph} = \left(\frac{G}{1000}\right).(I_{sc} + \alpha_{I_{sc}}.\Delta T) \quad (6)$$

Such that, G: Irradiance (W/m^2), $\Delta T = T_c$-$T_{c,ref}$ (Kelvin), T_c: driving cell heat (K), $T_{c,ref}$: Cell heat at STC = 25 + 273 = 298 K, I_{sc}: Short circuit current (A) at STC, αI_{sc}: Heat Coefficient of I_{sc} = 0.05% A/K) for suggested PV Module, I_{rs}: Reverse saturation diode current (A), εG: Physical band gap power (eV), (1.12eV for Si), k: Boltzmann constant 1.38x10^{-23} J/K, q: Electron Charge 1.602x10^{-19} C, and *Ns*: Sum of cells attached in series, for suggested PV cell = 60 cells.

1.3.2. The Controller of Voltage Source Converter (VSC)

When utilizing IGBTs and other high-power electronic devices, high-voltage direct current (HVDC) and high-voltage alternative current (HVAC) systems are connected via self-switching transformers known as voltage selected controllers (VSCs). VSCs don't require an AC system because they can turn on by themselves and generate AC voltage. Among the benefits of VSC are adjustable active and reactive power, AC voltage adjustment, and an appropriate installation size [16–28]. Figure 8 shows the VSC controller's phase locked loop (PLL) circuit design.

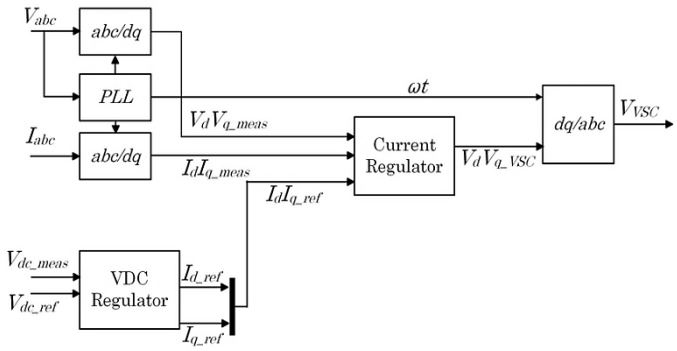

Figure 8. The MPPT circuit schematic for the VCS employing PLL controllers [16-28]

The phase-locked loop, PLL converts, v_{abc} to v_{dq}, and dynamically controls the rotational velocity of the *dq*-frame to maintain $v_q = 0$ [15-28]. The equation of the PLL operation might be written as:

$$v(t) = V_p.e^{(\omega t+\theta_0)} \quad (7)$$

Also,

$$v_d = V_p.\cos\left(\omega t + \theta_0 - \theta(t)\right) \quad (8)$$

$$v_q = V_p.\sin\left(\omega t + \theta_0 - \theta(t)\right) \quad (9)$$

By selecting $\theta(t) = \omega t + \theta_0$ the required outcome of having $v_q = 0$ is achieved. Although there are other PLL approaches that may be used, the most common structure in three-phase PLL implementations is the synchronous reference frame phase-locked loop, or SRF-PLL [15–28]. This was the portion that was used in this section. The SRF-PLL block diagram is shown in *figure 9*.

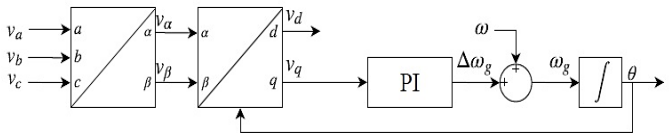

Figure 9. Demonstration of the SRF-PLL block diagram [15-28]

The input waveform v_q is fed towards the PI controller that results the angular frequency deviation $\Delta\omega.\omega = 2\pi f$ is next summer to this that is integrated into θ_0 at last. As it might be noticed in *figure 9*, it might be expressed by:

$$\theta = \int \omega_g dt = \omega t + \int \Delta\omega_g dt \quad (10)$$

The voltage selected controller (VSC), might be implemented also using pulse width modulation (PWM) strategy as shown in *figure 10* [15-28].

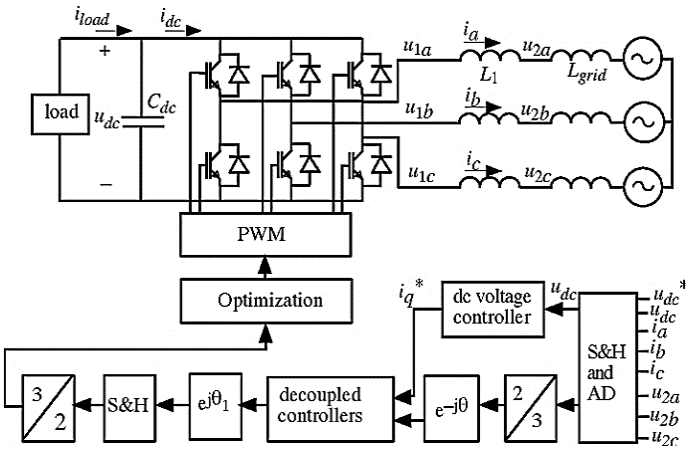

Figure 10. MPPT VCS with PWM controller circuit diagram [15-28]

FOREX Publication
Open Access | Rapid and quality publishing
International Journal of Electrical and Electronics Research (IJEER)
Research Article | Volume 13, Issue 2 | Pages 371-380 | e-ISSN: 2347-470X

2. LITERATURE REVIEW

Researchers have attempted to offer and recommend a variety of methods and strategies through assessment papers and scientific studies related to the subject of the advanced control model in the solar micro-grid utilizing intelligent estimating. To get a comprehensive understanding of the most recent advancements and updates on this subject, recent papers will be gathered and annotated with the title of the proposal to be presented. This will help to create a cohesive idea to address the evaluation problem and identify any issues or limitations found. Additionally, putting forward the recommendations that resulted. The PV bypass results in potential oscillations in the low-voltage transmission network. Together to eliminate this problem, another PID control scheme for ANFIS-based PV interface inverter with ANFIS-based monitored power limits in the panel frame of PV framework link is proposed in [15] [16]. Highlighted the viability of using a fuzzy controller to regulate DC transmission potentials in addition to suggesting a fuzzy logic-based control method for battery energy storage systems (BESS). A technique with a load module and a sustainable power supply is provided in [17] to control the energy storage scheme utilizing a fuzzy interface system (FIS). By improving the design and using an energy storage system (ESS), the suggested FIS was able to lower the fluctuations when compared to the standards-based control approach. A structural control based on climate metrics is proposed to reduce energy concern as well as increase the use of sustainable energy points to drive the panel in smaller than usual local grids [18]. A structured MPC control system is relied on addressing an optimum control obstacle limited to a specific instant-scheme horizon. Such proposed framework has also been contrasted with the rationale for ordinary rule-based control. Improvement in household solace constraints was observed with a typical 14.5% minimization in initial fossil power utilized. The rising entry of renewable energy sources has changed the movement of ideal models of energy frameworks. To adapt to these changes, executive authority frameworks have become larger, taking everything into account. For this reason, the evaluation area is full of studies on such frameworks. For example, many strategies use data to support executives' frameworks, traditional techniques [19], meta-heuristics [20, 21], and cybernetic reasoning techniques [22] with insightful model control [23]. Control plus energy trading-based implementation framework for micro-grid framework including of wind and PV with battery is proposed in [24]. The proposed energy management system (EMS) can be accessed regardless of the power supply. Such a framework can be synchronized against various references to reduce the grid energy throughout the operating time at any time when the load is greatest. For example, depending on the system, air is used as the initial energy supply, and photovoltaic energy is incorporated to manufacture the stable nature of the model in various climatic constraints. The battery unit is employed as a framework to store energy through boost power when there is a wealth of energy or potential interest in it [25]. A self-recovery algorithm that oversees ideal power flows to attain the lowest energy-dependent power costs and imposes highly predictable load utility charges along each source is offered in [26] as a way to monitor power supplies placed along small-scale power cores. For a grid architecture that includes wind and PV with battery, MPC with build-use and battery with value limits are anticipated to be necessary [27]. It was only logical to choose the right display and create the optimal capacity for the presentation of interest in addition to scanning here. A control architecture for MPPT based on an operationally ordered brain network is suggested. An EMS is set up using fuzzy logic to lower the power peak across the network. A fuzzy EMS is proposed based on the rationale of constraining oscillations with small grid-associated peak energies [28]. The traditional procedure for fuzzy genetic estimation has been proposed in articles [29]. Different GAs is used. The primary GA defines micro-grid power regulation as well as fuzzy principles, while the second GA aggregates fuzzy investment capabilities. The obscure main systems are also used to power the panel battery. The panel operation using a multi-objective particle swarm optimization procedure for a grid-tied micro-grid containing of a PV-FC battery Breeze Energy is proposed in [30]. It is planned to achieve maximum energy life along each source as well as reduce the cost of operating the micro-grid. Hybridization estimation is performed using PSO with Great Wolf Optimization (GWO) as well as the power of advance reservation of the day for which the panel technique was proposed [31]. Half the power of panel computation by modifying the standard+ rule of fuzzy selection framework against hierarchical genetic algorithm (HGA) is proposed in [32]. The fuzzy HGA calculation appears to be optimal compared to the traditional GA procedure, utilizing just 46.9% of the instructions within the standard condition. Through having a responsive and fewer disruptive logic controller, in which the overall control structure might be progressively employed using implanted electronics at minimal charge. The grid-tied micro-grid consists of wind power, PV, strong oxide power circuit (SOFC) supplies, and a BESS with two DCs practically identical to the AC loads [33]. A power based on a vague rationale is proposed to executives for a half frame with one half consisting of a PV-FC battery [34, 36]. Continuous long-term forecast data is used in the energy era as well. In a regulated system, multiport switches with attractive transmission are used to reduce potential phase changes. A nonlinear MPC method was proposed in [37]. A dummy neural network was used to evaluate the resistance square. The battery's state of charge (SOC), might be controlled according to the desired design to ensure potential safety. The associated network proposed an MPC-based EMS system in [38-40]. By increasing the wind energy employment with the battery, the energy reached the grid and the energy charging also decreased. To reduce the incoming power consumption along the network, using Gaussian interaction (GP) evaluation of the direct, on-board MPC operation is proposed in [41, 42]. Along GP, the PV power generation capacity is computed with the load demand capacity. An optimization-relied MPC strategy is utilized. In grid-connected frameworks, power inverters change the DC voltage PV yield into AC waveforms for the electrical power grid. The Air conditioner waveform should fulfill the sufficiency and frequency prerequisites at the purpose in like manner coupling (PCC) [43]. To lay out the association, phase-locked loop (PLL) methods or on the other hand synchronization algorithms are expected to synchronize the

FOREX Publication
Open Access | Rapid and quality publishing
International Journal of Electrical and Electronics Research (IJEER)
Research Article | Volume 13, Issue 2 | Pages 371-380 | e-ISSN: 2347-470X

inverter yields with the grid voltages [44]. Controlling the harmonic substance created by the exchanging of the inverter is likewise crucial semiconductors that are infused at the PCC [45]. As well as a synchronization algorithm and power quality control, there are extra capabilities, for example, against islanded protection, energy capacity regulation, dynamic power control, and grid support expected by ideas of value, congruity, and reliability. Such capabilities are required by grid codes [46]. The goal is that the grid-connected PV frameworks might enhance the energy framework elements by adding to blame moderation and guaranteeing soundness [47]. Moreover, monitoring, diagnostic, and prediction capabilities are a recent fad in high-power PV frameworks for monetary and ideal activity reasons [48]. To control current and voltage a two-loop control procedure is typically utilized. State of such construction is to isolate the dynamic response between the two rings. It should the internal ring quicker than the external ring. The normal design is to have an inward loop and an external voltage loop. PI controllers are normally utilized in both control loops, however they have weaknesses like restrictions on voltage regulation, clashes between control loops and little soundness areas [49]. To move along playing out a two-loop system, strong nonlinear controllers have been recommended. His last research several control techniques have been examined in double loop controllers, for example, dynamic disturbance rejection [50]. PI controllers [51-53], passivity-based control [54], predictive control [55, 56], droop control [57] and adaptive controllers [58]. Finally, in 2024, Firas M. Salbi et. al., [62] presented studying the minimum overhead and information check planning for procurement framework using Arduino LoRa. To gather data on PV current, battery, and voltage as well as PV efficiency, a mini-PV frame business strategy was put into action. The ALR was installed in the control room, which was about a kilometer away from the ALT, while the ALT was brought within the PVS region and successfully gathered data from the PV frame. Capturing data and displaying it on the chronic pasting screen was the aim of the ALR. At that point, the data was stored as a text document on the computer. Fifteen kilometers distant was the most severe access point. This frame cost around $150 CAD in total, which includes all of the standard frame components. It is found that the tire uses around 1.125 watts of electricity.

3. METHODOLOGY

Figure 11 introduces the proposed model simulation diagram to illustrate the operating approach.

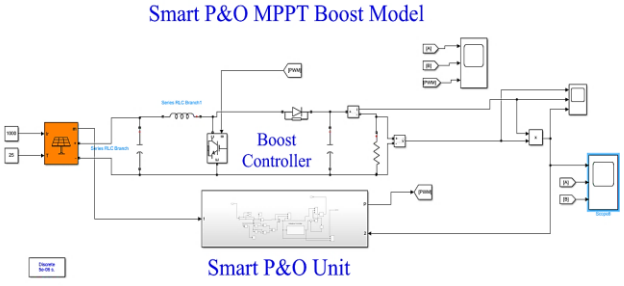

Figure 11. The suggested Simulink model block diagram

Photovoltaic cells, a boost controller, and a hybrid controller with an adaptive intelligent system are the three primary components that make up the simulated model seen in the above picture. The voltage and current signals from the photo cells unit will be evaluated and converted by the boost converter unit to improve the signal. One type of DC-to-DC power converter that raises voltage while decreasing current going from its input (source) to its consequence (weight) is a boost converter, also known as a move ahead converter. One power-saving component, such as an inductor, capacitor, or a combination of the two, and at least two semiconductors, a diode and a semiconductor, are included in this kind of switched-mode power supply (SMPS). The supply-side and burden-side channels of the converter are typically supplemented by capacitor-based channels to reduce potential waves. Power sources for the boost converter include coolers, batteries, solar chargers, DC generators, or any other functional DC source. When changing one DC voltage into another, the most popular technique is DC-to-DC transformation. It is referred to as a boost converter when the yield voltage of the DC-to-DC converter is higher than the source voltage. Sometimes called a "move forward converter," a boost converter "moves forward" the source voltage. Because P=VI and power regulation are required (display style P=VI), the result current is less than the source current. In the simulated model, the hybrid P&O with adaptive controller is the key element responsible for tracking the optimal or maximum power that can be taken from the model. Its two primary control units are the adaptive control unit and the P&O control unit. The overall power obtained will vary depending on how each controller responds to the differential change in PV voltage and current. This differential modification will be optimized until the model's output reaches its maximum power. *Figure 12* shows how the adaptive controller model is constructed.

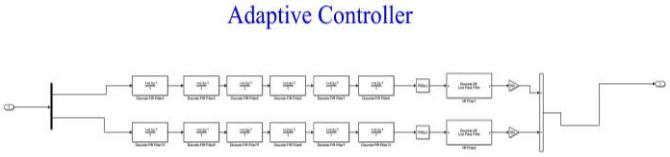

Figure 12. The construction of the adaptive controller technique

In order to guarantee that photovoltaic (PV) power displays operating in partial shadow (PSC) can consistently generate maximum power efficiently, this arrangement provides the highest converted cross-power point. The next tactic, known as MPPT, uses modified monitoring (intelligent controller) technology in conjunction with intelligent adaptive disturbance. The lucent emotion of every photoelectric cell section is activated, and light intensity sensors on-site can be replaced with less expensive voltage and current sensors to confirm set points. The adaptive technique uses background light intensity to predict the Global Maximum Power Point (GMPP) optimal voltage zones. The adaptive algorithm may detect a little change in photoelectric actuation, which is a portion of the P&O controller's differential change, when the hybrid controller and

FOREX Publication
Open Access | Rapid and quality publishing
International Journal of Electrical and Electronics Research (IJEER)
Research Article | Volume 13, Issue 2 | Pages 371-380 | e-ISSN: 2347-470X

smart controller work together, improving triad tracking. The MatLab2023b Simulink toolbox has been used to create the simulated structure of the proposed hybrid smart P&O adaptive controlling approach system for improving the inverter characteristics of the PV system.

The concept behind the suggested model's functioning mechanism will next be examined and explained in accordance with the procedures involved in its execution, from creating and processing the data set to achieving the desired outcomes.

Figure 13 may show the flow chart for the design and implementation phases of the suggested model for the electrical distribution network's smart controller.

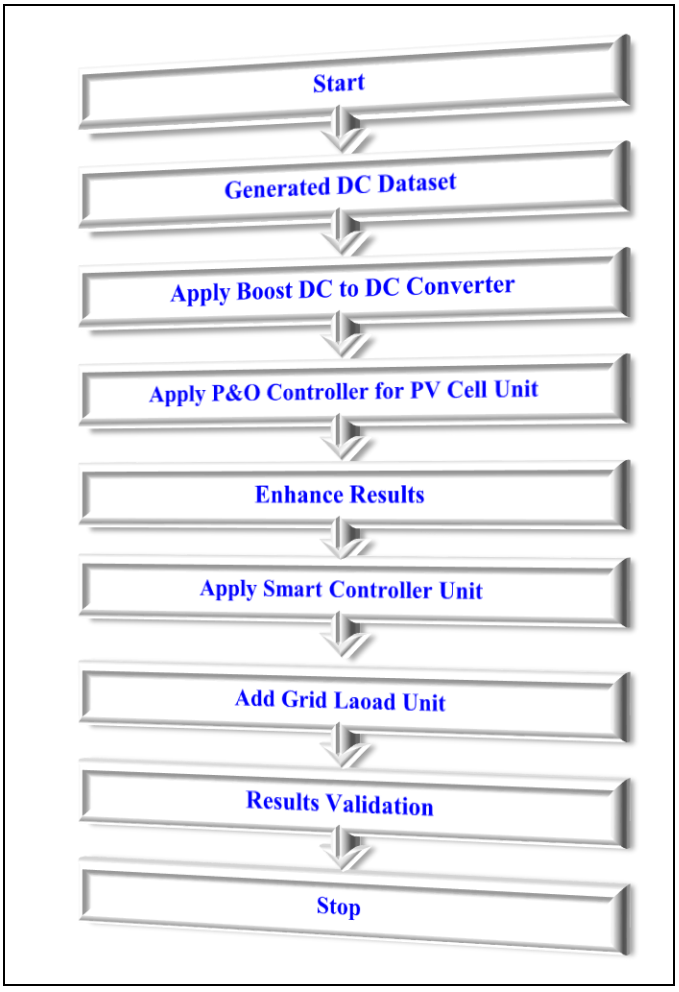

Figure 13. The flow chart for the design and implementation units in the proposed model of the smart controller for the electrical distribution network

The software starts by defining the utilized data set, which was produced by using a controlled photovoltaic unit and a battery support unit to prepare the DC voltage and current feeding the system, according to the specifics of the flow chart displayed in *figure 13*. The next step is the installation of the boost DC to DC converter unit, which is managed by the smart controller unit, the most crucial component of the project and reflects voltages ranging from low to high. Afterward, keeping an eye on the model and verifying the outcomes. The program is then terminated after the procedure is repeated until MPPT is reached and confirmed.

Table 1 provides a summary of the design parameters used to create the simulation scheme for the implementation of the recommended model's simulation structure.

Table 1. The design parameters utilized to set the implement the simulation model

Design Components	Rs (Ohm)	C_1 (F)	R_1 (Ohm)	L_1 (H)	C_2 (F)	Rp (Ohm)
Value1	200	$10e^{-6}$	10	$2e^{-3}$	$20e^{-6}$	1000
Value2	500	$20e^{-6}$	15	$5e^{-3}$	$50e^{-6}$	2000

4. RESULTS AND DISCUSSION

Employing the MatLab2023b Simulink toolbox, the simulated structure of the proposed PV system inverter characteristics enhancement employing hybrid smart P&O adaptive regulating approach system has been put into practice. The design parameters used to create the simulation scheme are described in *table 1* and have been applied to the simulation structure of the proposed model. The voltages, currents, and power signals of the produced PV cells are shown in *figure 14*. It is clear through the outcomes that the PV voltage and current are unsteady, and the achieved PV energy is varying under the intended ultimate and getting close to unstapled values.

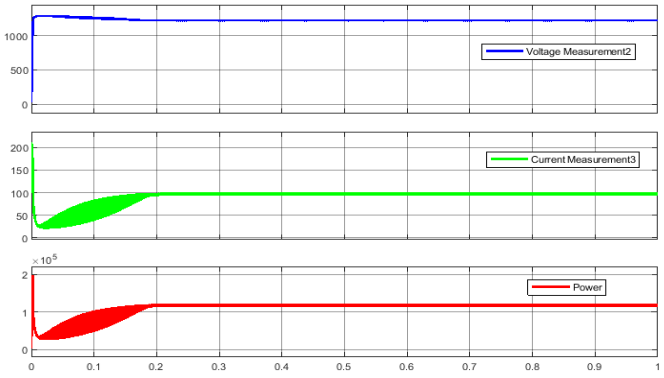

Figure 14. The produced PV cells voltages, currents, and power waveforms

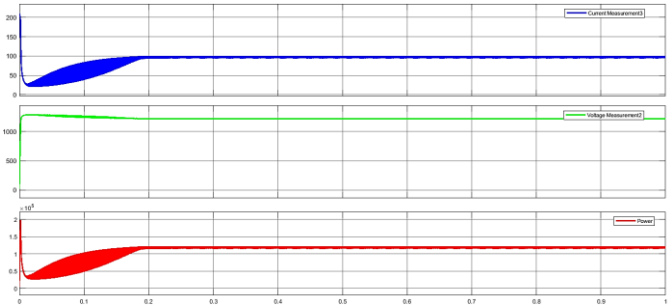

Figure 15. The resulting signals from the ANN controller

FOREX Publication
Open Access | Rapid and quality publishing
International Journal of Electrical and Electronics Research (IJEER)
Research Article | Volume 13, Issue 2 | Pages 371-380 | e-ISSN: 2347-470X

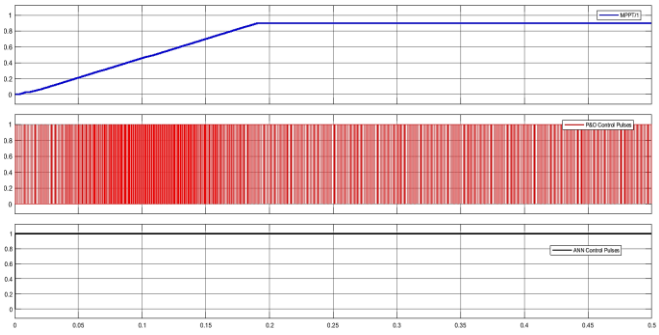

Figure 16. Output signals from the P&O controller compared with the adaptive controller

On the other hand, the values of produced current are further alternating down 20 A, whereas the potential is reaching to more than 1000 V because the cells are connected in series. Now, the resulting signals along the adaptive controller are displayed in *figure 16*. The upper red colored signal is the controlled power signal at the result of the ANN controller, and the lower blue colored signal is the resulting controlled voltage signal. Next, the output waves from the P&O controller compared with the adaptive controller are illustrated in *figure 15*. The upper blue colored signal is the P&O controller signal before comparison with saw tooth pulses and is represents the variations of the differential changes between voltage and current of the PV cells after forcing the circuit to produce the maximum power. The second red colored signal is the output pulses obtained from the P&O controller after comparing the differential varied blue signal with the saw tooth pulses to get the controlling pulses to the boost converter. At last, the third black colored signal is the output pulse from the pulse width modulator (PWM) after the adaptive controller. This signal also represents the observation of the fractional alternation in the PV potential against currents entered to the adaptive algorithm, in which the maximum power will be achieved. Such controlling pulses will be applied to the boost converter to optimize the entered PV cells DC voltage and current signals and achieve maximum power tracking value MMPT as presented in *figure 17*.

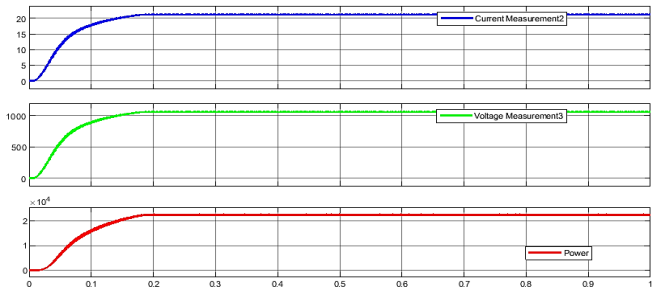

Figure 17. Resulting maximum power tracking point MMPT signals using hybrid P&O-adaptive controller

It is obvious from *figure 17* that, the hybrid controller operates to obtain the best MMPT results as the power reaches to more than 20 KW as presented with the red colored curve. This has been achieved by tracking the maximum current and voltage of the PV cells utilized in the simulation so that, the final current reaches to 22 Amp as shown in the blue colored curve, with final overall voltage of 1150 V. By reviewing the results achieved from implementing the suggested system, one could find that the implementation of smart adaptive algorithms for PV MPPT with P&O controllers will assist in providing a proper and appropriate MPPT results with high DC to ac conversion. In order to complete the idea of research and thesis, one could compare the results obtained from the simulation of the proposed technique along the outcomes of the similar scheme, but utilizing the traditional P&O type controller. Using the similar design parameters implemented with the hybrid model those illustrated in *table 1*, the resulting MPPT signals are introduced in *figure 17*. As it is clear from the obtained results of the simulated model using typical P&O controller that, the final tracking power is only 5000 W which is much less than that obtained by the hybrid model. Also, the achieved final voltage and current are resulting with lower values of 500 V and 10 A. Moreover, the same PV boost converter simulation model is employed but with ANN control technique without applying P&O strategy. Applying the similar design parameters implemented with the hybrid model those illustrated in *table 2*, the resulting MMPT signals are displayed in *figure 18* and *19*.

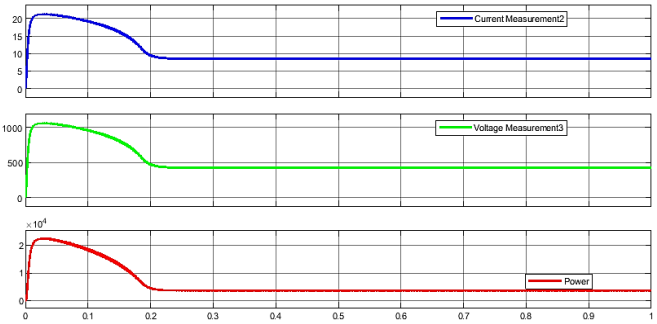

Figure 18. Resulting maximum power tracking point MMPT signals using Boost strategy

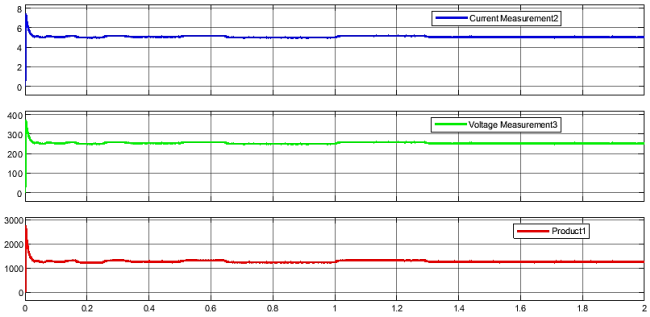

Figure 19. Resulting maximum power tracking point MMPT signals using adaptive smart controller

As observed from the achieved results of the simulated model utilizing typical adaptive controller that, the final tracking power is only 1000 W which still much less than that obtained by the hybrid model. Also, the achieved final voltage and current are resulting with lower values of 220V and 5A. By such results, the final conclusion is clear that the simulation model with the hybrid fly Back-ANN controller has better MMPT performance be 4 times that obtained using only P&O control.

FOREX Publication
Open Access | Rapid and quality publishing
International Journal of Electrical and Electronics Research (IJEER)
Research Article | Volume 13, Issue 2 | Pages 371-380 | e-ISSN: 2347-470X

The comparison of the outcomes for the three methods is summed up in *table 2*. Additionally, the outcomes of previous scientific research and papers were contrasted with the model we provide in this thesis. *Table 2* presents a concise comparison between our suggested model and those offered by recently published research.

Table 2. An overview of the differences in the outcomes of the three approaches

Control Strategy	D.C. Current I (Ampere)	D.C. Potential V (Volts)	MMPT P (Watt)
Adaptive	5	220	2000
P&O	10	500	5000
Hybrid	20	1250	25000

5. CONCLUSION

This study used a hybrid P&O adaptive smart controller with smart operation to analyze and evaluate the impacts of combining two controllers on the boost converter PV cells framework. Highest power point tracking (MPPT) refers to the optimal potential such that the grids attain the highest energy along the minimal expenses.

• To provide the framework with partially shadowed direct current, effective photovoltaic (PV) prison cells have been used as steady DC power sources. Two types of boost controllers have been used to simulate and analyze the projected PV cells model.

• According to the simulation findings, out of the two different controllers, the hybrid P&O-adaptive controller offers the best maximum power point tracking (MPPT).

• The proposed model generates a 25 KW MPPT power, which is frequently superior to the adaptive controller and P&O technology separately.

Conflicts of Interest: The authors declare no conflict of interest or disclose any conflicts of interest.

REFERENCES

[1] R. Liu, B. Yang, E. Zio, and X. Chen, "Artificial intelligence for fault diagnosis of rotating machinery: A review," Mech. Syst. Signal Process., vol. 108, pp. 33–47, 2018.

[2] H. Shao, H. Jiang, L. Ying, and X. Li, "A novel method for intelligent fault diagnosis of rolling bearings using ensemble deep auto-encoders," Mech. Syst. Signal Process., vol. 102, pp. 278–297, 2018.

[3] S. Satpathy, S. Debbarma, A. S. C. Sengupta, and B. K. D. Bhattacharyya, "Design an FPGA, fuzzy based, insolent method for predicting multi-diseases in a rural area," J. Intell. Fuzzy Syst., vol. 37, no. 5, pp. 7039–7046, 2019.

[4] Q. Wu et al., "Incipient Fault Diagnosis Method via Joint Adaptive Signal Decomposition," in IEEE Sensors Journal, vol. 24, no. 15, pp. 24308-24318, 1 Aug.1, 2024, doi: 10.1109/JSEN.2024.3414299.

[5] Liu, Qiang, Liu, Songyong, Dai, Qianjin, Yu, Xiao, Teng, Daoxiang, Wei, Ming, Data-Driven Approaches for Diagnosis of Incipient Faults in Cutting Arms of the Roadheader, Shock and Vibration, 2021, 8865068, 15 pages, 2021.

[6] P. Subbulakshmi, "Mitigating eavesdropping by using fuzzy based MDPOP-Q learning approach and multilevel Stackelberg game theoretic approach in wireless CRN," Cogn. Syst. Res., vol. 52, pp. 853–861, 2018, doi: 10.1016/j.cogsys.2018.09.021.

[7] H. Chen, B. Jiang, S. X. Ding, N. Lu and W. Chen, "Probability-Relevant Incipient Fault Detection and Diagnosis Methodology with Applications to Electric Drive Systems," in IEEE Transactions on Control Systems Technology, vol. 27, no. 6, pp. 2766-2773, Nov. 2019, doi: 10.1109/TCST.2018.2866976.

[8] S. Neelakandan, "An automated exploring and learning model for data prediction using balanced CA-SVM," J. Ambient Intell. Humaniz. Comput., vol. 12, no. 5, 2020, doi: 10.1007/s12652-020-01937-9.

[9] Y. Wang, Z. He, and Y. Zi, "Enhancement of signal denoising and multiple fault signatures detecting in rotating machinery using dual-tree complex wavelet transform," Mech. Syst. Signal Process., vol. 24, pp. 119–137, 2010.

[10] S. Satpathy, S. Das, and S. Debbarma, "A new healthcare diagnosis system using an IoT-based fuzzy classifier with FPGA," J. Supercomput., vol. 76, no. 8, pp. 5849–5861, 2020, doi: 10.1007/s11227-019-03013-2.

[11] Sai, NV Midhun, M. S. Saravanan, and P. Subramanian. "A novel network packet loss detection framework using random forest algorithm over support vector machine learning algorithms to improve accuracy." 2022 International Conference on Knowledge Engineering and Communication Systems (ICKES). IEEE, 2022.

[12] Raju, K. Sagar, and V. Amudha. "Early Detection and Quantification of Osteoarthritis Severity in Knee Using Support Vector Machine with Improved Accuracy Compared to Convolutional Neural Network." 2023 Eighth International Conference on Science Technology Engineering and Mathematics (ICONSTEM). IEEE, 2023.

[13] R. R. Bhukya, B. M. Hardas, T. Ch., et al., "An automated word embedding with parameter tuned model for web crawling," Intell. Autom. Soft Comput., vol. 32, no. 3, pp. 1617–1632, 2022.

[14] Z. Chen, K. Gryllias, and W. Li, "Mechanical fault diagnosis using convolutional neural networks and extreme learning machines," Mech. Syst. Signal Process., vol. 133, p. 106272, 2019.

[15] S. Guo, T. Yang, W. Gao, and C. Zhang, "A novel fault diagnosis method for rotating machinery based on a convolutional neural network," Sensors, vol. 18, no. 5, p. 1429, 2018.

[16] W. Gong et al., "A novel deep learning method for intelligent fault diagnosis of rotating machinery based on improved CNN-SVM and multichannel data fusion," Sensors, vol. 19, no. 7, p. 1693, 2019.

[17] M. Z. Hasan and F. Al-Turjman, "Optimizing multipath routing with guaranteed fault tolerance in Internet of Things," IEEE Sens. J., vol. 17, no. 19, pp. 6463–6473, Oct. 2017, doi: 10.1109/JSEN.2017.2739188.

[18] W. Jiang, C. Wang, J. Zou, and S. Zhang, "Application of deep learning in fault diagnosis of rotating machinery," Processes, vol. 9, no. 6, p. 919, 2021.

[19] X. Wu, Y. Zhang, C. Cheng, and Z. Peng, "A hybrid classification autoencoder for semi-supervised fault diagnosis in rotating machinery," Mech. Syst. Signal Process., vol. 149, p. 107327, 2021.

[20] R. M. Souza et al., "Deep learning for diagnosis and classification of faults in industrial rotating machinery," Comput. Ind. Eng., vol. 153, p. 107060, 2021.

[21] Alamanda, Sophia, et al. "Machine Learning-Based Fault Diagnosis for Rotating Machinery in Industrial Settings." 2024 Ninth International Conference on Science Technology Engineering and Mathematics (ICONSTEM). IEEE, 2024.

[22] H. Shaodong, D. Ziyang, C. Junsheng, and J. Hongkai, "Intelligent fault diagnosis among different rotating machines using novel stacked transfer auto-encoder optimized by PSO," ISA Trans., vol. 105, pp. 308–319, 2020.

International Journal of
Electrical and Electronics Research (IJEER)
Research Article | Volume 13, Issue 2 | Pages 371-380 | e-ISSN: 2347-470X

[23] A. G. Howard et al., "Mobilenets: Efficient convolutional neural networks for mobile vision applications," arXiv preprint arXiv:1704.04861, 2017.

[24] Y. Fan, C. Zhang, Y. Xue, and J. Wang, "A bearing fault diagnosis using a support vector machine optimized by the self-regulating particle swarm," Shock Vib., vol. 2020, Article ID 9096852, 11 pages, 2020, doi: 10.1155/2020/9096852.

[25] M. R. Kumar, V. C. S. Rao, R. Anand, and H. Singh, "Interpretable filter based convolutional neural network (IF-CNN) for glucose prediction and classification using PD-SS algorithm," measurement, vol. 183, 2021, doi: 10.1016/j.measurement.2021.109804.

[26] C. Al-Atroshi, V. K. Nassa, B. Geetha, S. Neelakandan, et al., "Deep learning-based skin lesion diagnosis model using dermoscopic images," Intell. Autom. Soft Comput., vol. 31, no. 1, pp. 621–634, 2022.

[27] P. Boyapati, S. Neelakandan, A. A. A. Akeji, A. K. S. Pundir, and R. Walia, "LSGDM with biogeography-based optimization (BBO) model for healthcare applications," J. Healthc. Eng., vol. 2022, Article ID 2170839, 11 pages, 2022, doi: 10.1155/2022/2170839.

[28] A. Subasi, "Medical decision support system for diagnosis of neuromuscular disorders using DWT and fuzzy support vector machines," Comput. Biol. Med., vol. 42, no. 8, pp. 806–815, 2012.

[29] AlShorman, Omar, et al. "Advancements in condition monitoring and fault diagnosis of rotating machinery: A comprehensive review of image-based intelligent techniques for induction motors." Engineering Applications of Artificial Intelligence 130 (2024): 107724.

[30] J. Gu and S. Lu, "An effective intrusion detection approach using SVM with naïve Bayes feature embedding," Comput. Secur., vol. 103, p. 102158, 2021.

[31] V. Savithiri and S. Gomathi, "Fault Detection Algorithms for Improving Accuracy in Solar PV System," 2024 9th International Conference on Communication and Electronics Systems (ICCES), Coimbatore, India, 2024, pp. 203-207, doi: 10.1109/ICCES63552.2024.10859624.

[32] S. P. Kala, P. Kumar S, G. Meerimatha, M. Almusawi and S. Gurumoorthy, "Smart Monitoring and Diagnostics for Fault Detection in Power Plant Equipment," 2024 Third International Conference on Distributed Computing and Electrical Circuits and Electronics (ICDCECE), Ballari, India, 2024, pp. 1-4, doi: 10.1109/ICDCECE60827.2024.10548401.